Solid Freeform Fabrication 2019: Proceedings of the 30th Annual International
Solid Freeform Fabrication Symposium – An Additive Manufacturing Conference
Reviewed Paper

Effects of Unit Cell Size on the Mechanical Performance of Additive Manufactured Lattice Structures

Arash Soltani-Tehrani[1, 2], Seungjong Lee[1, 2], Mohammad Reza Vaziri Sereshk, Nima Shamsaei[1, 2, *]

[1]National Center for Additive Manufacturing Excellence (NCAME), Auburn University, Auburn, AL 36849
[2]Department of Mechanical Engineering, Auburn University, Auburn, AL 36849
* Corresponding author: shamsaei@auburn.edu

Abstract

Lattice structures are generated through the repetition of smaller structures, defined as unit cells. These structures are popular alternatives for bone implants due to the potential to adjust the stiffness. However, in some applications, there are volume and mass constraints that cannot be exceeded. Therefore, to match the lattice structure's stiffness to that of the natural bone, unit cell sizes should be altered. In this study, the effects of different unit cell sizes, on the compression behavior of lattice structures fabricated from 316L stainless steel (SS) via laser beam powder bed fusion (LB-PBF) are studied through finite element analysis (FEA) while the volume and mass are kept constant and results of which, are validated by experiments. It was found that energy absorption capability and stiffness of lattice structures can increase with decreasing the size while the volume and mass are kept constant. The lattice structure with smaller unit cell dimensions tolerated a relatively higher maximum force for the same amount of displacement.

Keywords: Lattice Structures; Laser Beam Powder Bed Fusion (LB-PBF); Stainless Steels; Stiffness; Bone Implants

Introduction

Lattice structures are porous structures which are generated through the repetition of smaller structures defined as unit cell [1]. Unit cells are also formed by the connection of struts with different cross-section shapes such as rectangular, circular and hexagonal [1]. Some common unit cells are BCC, FCC, diamond, and gyroid [1–4]. Therefore, different mechanical properties can be expected by the different unit cell types, which makes lattice structures suitable for many applications such as medical implants, energy absorption, and light-weighting applications [1,5–9]. However, fabrication of lattice structures via traditional manufacturing methods (i.e., cutting, machining, brazing, and welding) is difficult or even impossible.

Nowadays, producing lattice structures with different additive manufacturing (AM) technologies such as laser beam powder bed fusion (LB-PBF) is very common due to more design freedom in these manufacturing methods. In LB-PBF, parts are fabricated in a layer-wise fashion from the powder feedstock with minimal interference of human in manufacturing. Different computer-aided design (CAD) files can be imported directly to the manufacturing machine for production. In addition, processing many materials such as titanium alloys (e.g., Ti-6Al-4V),

aluminum alloys (e.g., AlSi10Mg), and stainless steel (SS) alloys (e.g., 316L SS) [1–6,9–14] has been made possible through this type of manufacturing.

Although manufacturing lattice structures with very complex geometries and from different materials have been possible via LB-PBF, there are still some challenges, which have hampered their widespread use in different applications. For example, when the lattice structure is used as a bone implant, stress shielding can occur due to the stiffness mismatch between the bone and implant [15]. Fatigue failure can also happen in implants since they are usually exposed to different loading types such as compression-compression and compression-tension [1]. The relatively high surface roughness after fabrication via LB-PBF can also be detrimental in some applications [16]. These challenges make studying different lattice structures very important. Many studies have been performed regarding lattice structures fabricated with different unit cell types. For example, Yanez et al. [14] studied gyroid lattice structures fabricated via electron beam melting (EBM) in normal- and deformed-shape conditions. Higher stiffness and strength were observed for deformed gyroids under compression while normal gyroids showed higher stiffness and strength under torsion.

Van Hooreweder et al. [17] studied different post-processing treatments including hot isostatic pressing (HIP) and chemical etching in order to decrease the surface roughness inherent to LB-PBF. Chemical etching was observed to increase fatigue strength of Ti-6Al-4V samples. In addition, further improve in fatigue strength was observed by HIP specially in the high-cycle-fatigue (HCF) region. Lieteart et al. [18] studied different loading combinations including tension-tension, compression-tension, and compression-compression to investigate the fatigue behavior of lattice structures. It was observed that due to the presence of local mean tensile stress in tension-tension and compression-compression loading types, lower fatigue life can be yielded compared with compression-tension loading. Plessis et al. [12] showed that different unit cell types can also result in different mechanical properties while the volume fraction is constant. In this study, diagonal and rhombic lattice structures fabricated from Ti-6Al-4V via LB-PBF with a 50% volume fraction under compressive loading were investigated [12]. Relatively higher ultimate compressive stress (UCS) and Young's modulus were observed for the rhombic lattice structure compared with diagonal. μCT simulations also revealed that failures started from high-stress regions which were mostly located at the nodes.

In addition to the aforementioned challenge, there are sometimes mass and volume constraints as well for specific applications. In order to obtain the desired mechanical properties (e.g., stiffness) and keep constant mass and volume, unit cell dimensions need to be altered. In this study, effects of unit cell dimensions on the mechanical behavior of lattice structures under static loadings will be investigated via finite element analysis (FEA). The results of FEA will also be verified by experimental quasi-static compression tests, and final conclusions will be made based on the results.

Finite Element Simulations

Lattice structures were analyzed with ABAQUS in order to study the mechanical response under monotonic compression. A linear tetrahedral element (C3D4) was used to mesh the structures. The mesh was also verified to rule out the mesh-dependency of the results. Both elastic and plastic properties were selected for the material according to 316L SS properties obtained from [19]. A 5-mm displacement and an ENCASTRE boundary conditions were applied on the top and

bottom plates of lattice structures, respectively. Von Misses stress, displacement, reaction forces, and strain were obtained using FEA in lattice structures.

Experimental Program

Different lattice structures were fabricated from different BCC4 unit cells via Renishaw AM250, an LB-PBF manufacturing machine, in an argon atmosphere (see **Figure 1**(a)). The powder feedstock used in this study was argon-atomized 316L SS fabricated by LPW Technology Ltd with an initial particle size distribution of 15-45 µm. The overall volume of lattice structures was designed with dimensions of 14.4 mm × 14.4 mm × 14.4 mm. Lattice structures were fabricated with 6, 8, and 10 unit cells in each direction with different unit cell lengths and strut diameters in order to keep volume and mass constant. Two plates with a thickness of 0.5 mm were also located on top and bottom of lattice structures to uniformly distribute the compressive load. As shown in **Figure 1**(b), lattice structures with 6, 8, and 10 unit cells in each direction were defined as BCC6, BCC8 and BCC10, respectively.

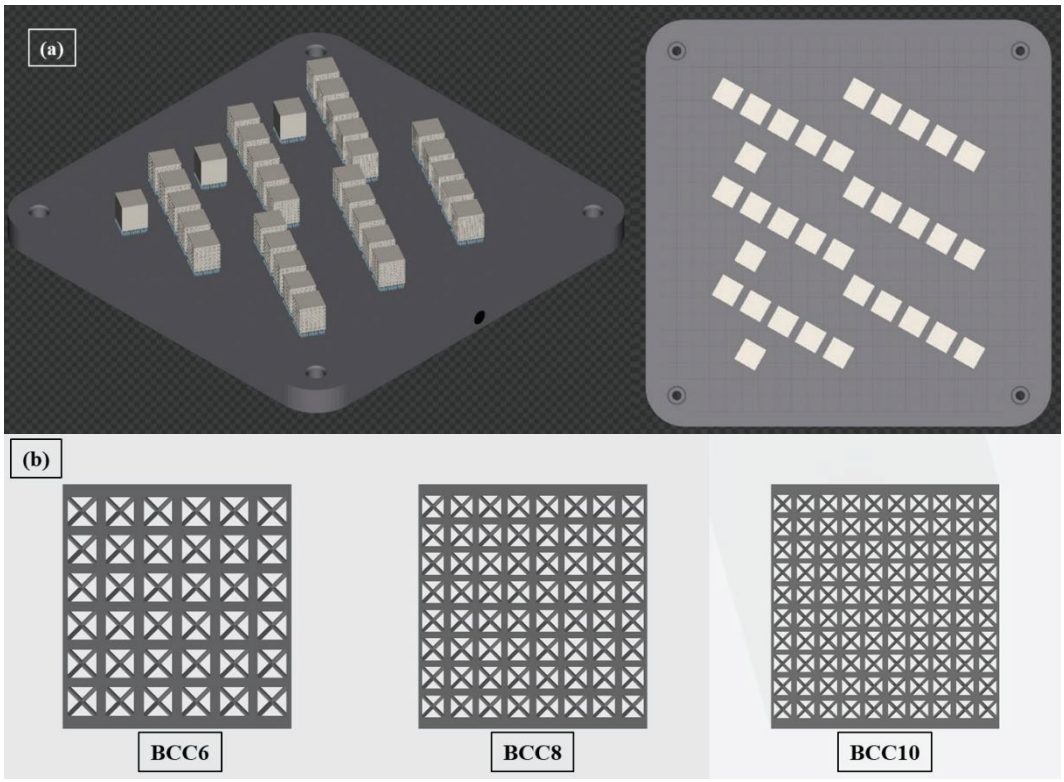

Figure 1 (a) isometric (left) and top (right) view of the build plate, and (b) front view of BCC6, BCC8, and BCC10

After fabrication, specimens were removed from the build plate. They were cleaned completely using an ultrasonic cleaner to ensure removal of loose powder particles entrapped within the lattice structures or on the surface. Parts were measured and tested without any additional post-processing treatment. Quasi-static compression tests were performed via MTS 810 servo-hydraulic system with a displacement rate of 0.015 mm/s. Tests were performed in a displacement-controlled mode and continued to 5 mm. The tests were stopped if the applied force

reached 70 kN and considered as failed. To verify the results, three tests were performed for each condition.

Results and discussion

Lattice structures including BCC6, BCC8, and BCC10 were analyzed using finite element method. All lattice structures went through 5 mm displacement (see **Figure 2**). As seen in this figure, the BCC6 lattice structure under monotonic compression deforms with a barreling shape. In addition, the first row of unit cells under compression have the highest amount of displacement leading to collapse of the first row prior to other rows. This behavior continues in the aforementioned lattice structure until all the rows collapse and there is no unit cell to absorb the energy. In this stage, densification in lattice structure happens which comes with a sudden increase in stress and final failure of the specimen [1]. Similar behavior in displacement from FEA was observed for BCC8 and BCC10. However, it was observed that BCC8 and BCC10 can absorb more energy compared with BCC6 lattice structure. It seems that the final failure in BCC10 happens at a relatively higher strain compared with BCC8 and finally BCC6. Therefore, it is expected that for the same amount of displacement, BCC10 requires more applied force compared with BCC8 and BCC6, respectively. This behavior can be explained by the existence of more unit cells to absorb the applied energy.

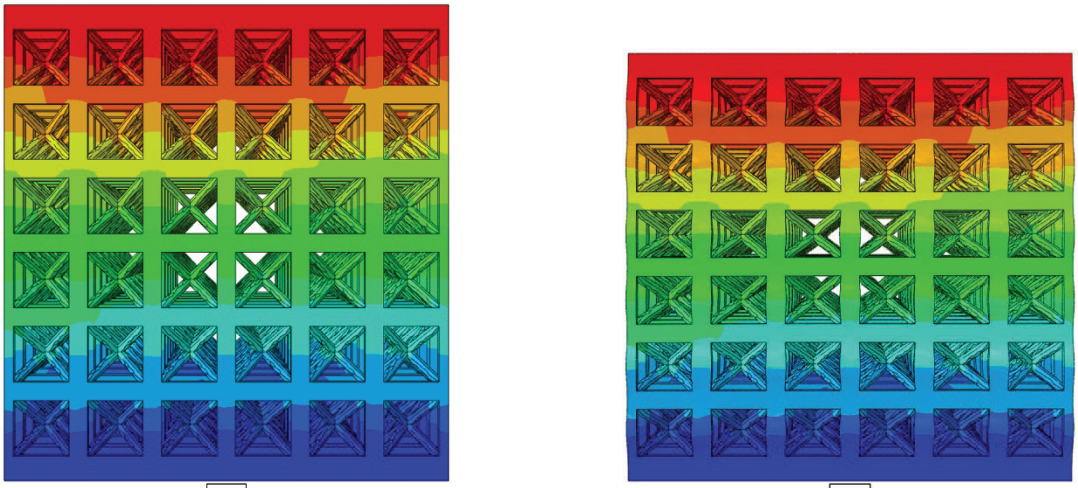

Figure 2 BCC6 lattice structure in (a) before and (b) after 5 mm displacement

As seen in **Figure 3**, Von Misses stress within the BCC6, 8, and 10 lattice structures is shown for 5 mm displacement. No failure was observed by deforming the lattice structure for 5 mm. In addition, it can be observed that a relatively smaller amount of stress is applied on the vertical struts of BCC10 followed by BCC8 compared with BCC6. This behavior was also verified by looking at the strain results. It was observed that the amount of strain at the vertical struts of BCC6 lattice structure is at the highest. This decrease in stress and strain was also observed for the internal diagonal struts of each unit cells, however, it was more significant for the vertical struts. Moreover, as seen in this figure, the horizontal struts of all lattice structures are under tension due

to bending stress at these struts although the structure is under compression. Therefore, horizontal struts under relatively higher tension deform more in the perpendicular direction to loading, which contributes to the higher energy absorption of BCC10 lattice structure followed by BCC8 and BCC6.

The reaction forces from the top plate were also plotted for deformed lattice structures using FEA, and it was observed that the maximum reaction force in BCC6, BCC8, and BCC10 are 539 kN, 402 kN, and 280 kN, respectively. However, there were relatively higher number of regions with maximum force in the BCC10. This shows that by increasing the number of unit cells, the applied force, and consequently, stress is divided into more unit cells which decrease the maximum amount of stress. Therefore, smaller displacement happens at BCC10 unit cells for the same amount of applied stress.

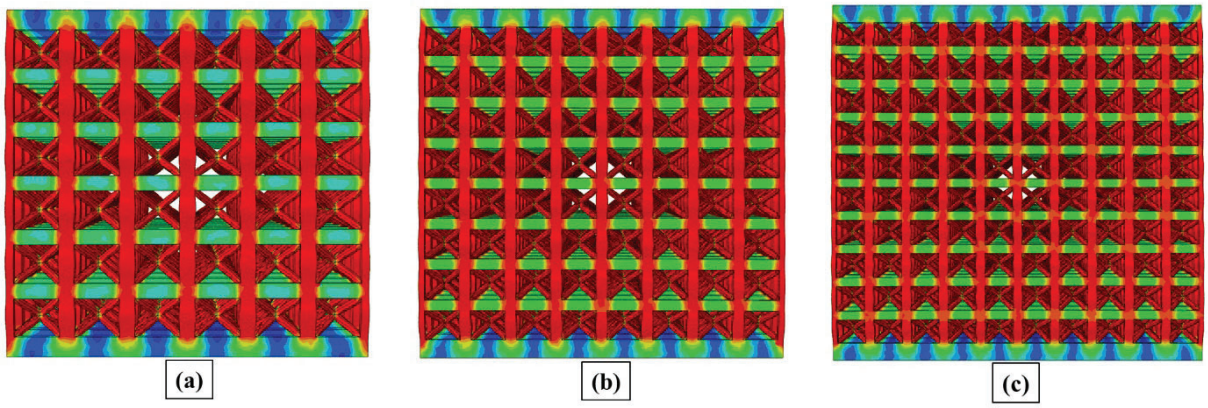

Figure 3 Von Misses stress shown in (a) BCC6, (b) BCC8, and (c) BCC10 lattice structures after 5 mm displacement

In addition to numerical simulations, all lattice structures with different number of unit cells in each direction were tested under monotonic compressive loading. The force-displacement curves are shown in **Figure 4**. As shown in this figure, all lattice structures are first deformed with a linear elastic behavior, which is then followed by a plateau region where force gradually increases with permanent deformation. This behavior conforms with the literature [20]. In these studies, the third regime (i.e., densification) where a sudden increase in force/stress happens for a relatively small increment of displacement, is also shown. However, in the current study, tests were stopped at 5 mm, and the third regime was not shown. It can be observed from the figure that BCC8 and BCC10 were almost comparable in the elastic region. However, BCC10 showed superior strength after the first yield.

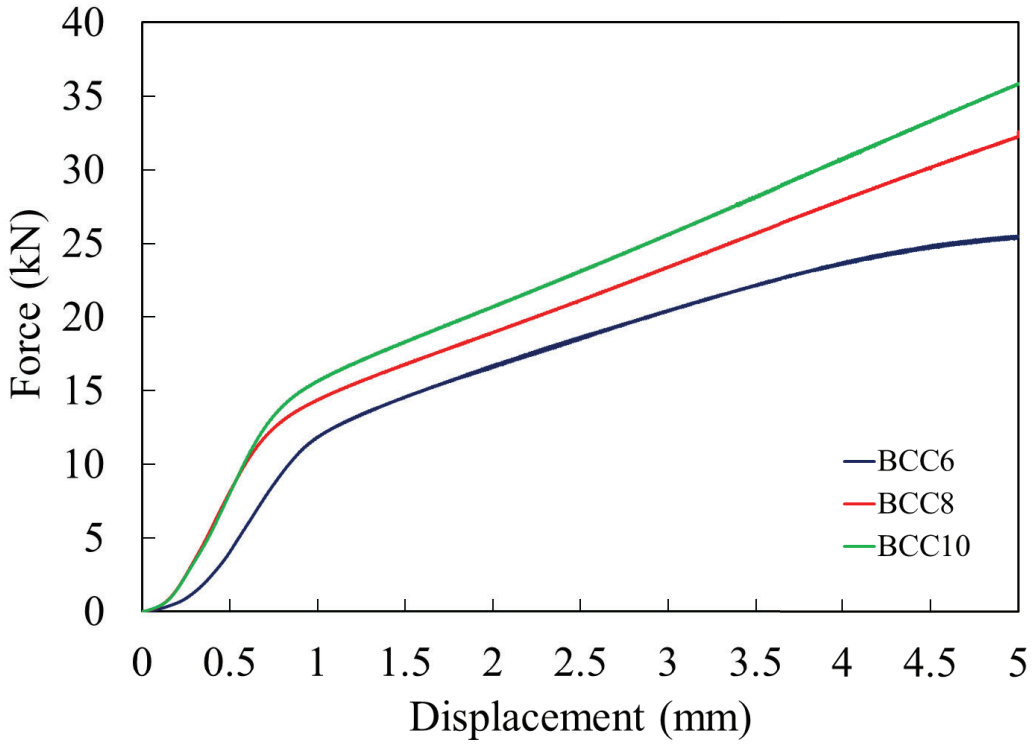

Figure 4 Force-displacement curves for BCC6, BCC8 and BCC10 lattice structures under displacement-controlled compressive loading for 5 mm deformation

All lattice structures deformed comparable to each other, and deformation started with the failure of unit cells row by row. In addition, all the specimens deformed with a barreling shape, which was also observed in FEA results (see **Figure 5**). Stiffness was calculated based on the slope of the force-displacement curve in the elastic region for each lattice structure, and it was found to be 18.4 N/mm, 22.9 N/mm, and 24.9 N/mm for BCC6, BCC8, and BCC10, respectively. Therefore, stiffness was increased by increasing the number of unit cells and decreasing the dimensions (i.e., unit cell length and strut diameter). Since in open-celled structures (i.e., lattice), bending deflection is proportionate to force, length, Young's modulus, and moment of inertia [21], it can be concluded that stiffness is directly correlated with Young's modulus and moment of inertia, and inversely correlated with length. Therefore, by increasing the number of unit cells, and consequently, decreasing the length of unit cells, an increased stiffness value can be expected.

In all deformed lattice structures, deformation started from the nodes between each two rows. This behavior conforms well with the FEA where a relatively higher Von Misses stress was shown at these nodes. It was observed that stress is relatively higher in vertical struts of BCC6 while by increasing number of unit cells, a smaller amount of stress was applied on these struts. Although the lattice structure is tested under compressive loading, there was also tensile stress available in the horizontal struts due to the bending moment. Therefore, unit cells fail at nodes where horizontal and vertical struts are connected to each other, and this behavior continues until the part is completely failed.

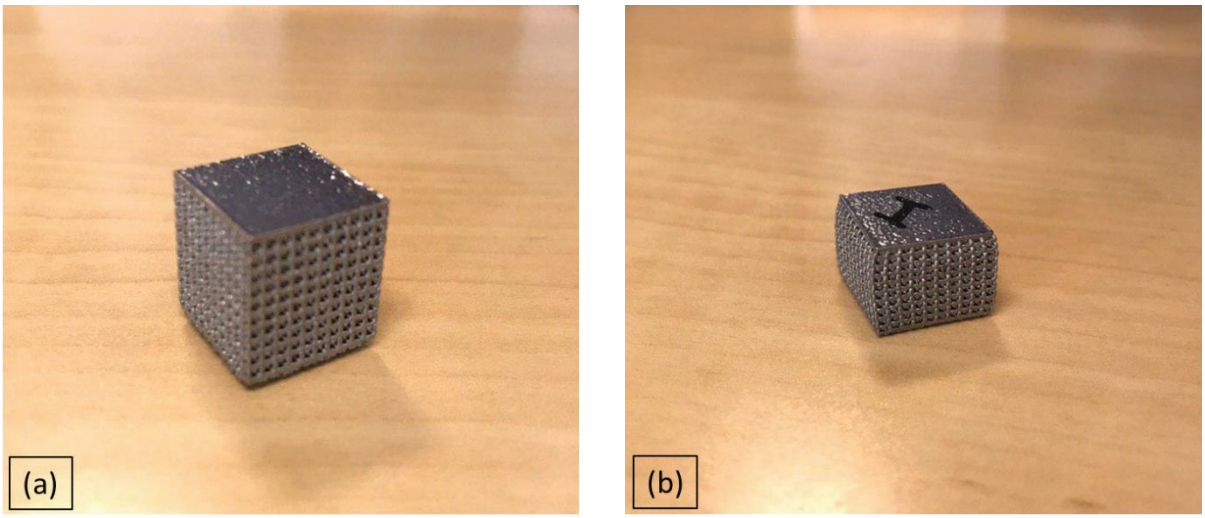

Figure 5 BCC10 lattice structure: (a) before and (b) after 5 mm displacement

Conclusions

In this study, three different lattice structures fabricated from BCC4 unit cell with different dimensions (i.e., unit cell length and strut diameter), were fabricated via LB-PBF from 316L SS while the volume and mass were kept constant. Finite element analysis was used to investigate the behavior of these structures under compression and to find the locations for maximum stress. In addition, monotonic behavior of these structures was obtained under compressive loading with a displacement-controlled program, where deformation was set to be 5 mm. Based on the observations and results, following conclusions can be made:

1. BCC4 lattice structures represented good strength and stiffness, which make them suitable for many medical applications [22].
2. The monotonic behavior of lattice structures under compressive loadings did not alter significantly with the change of unit cell dimensions, while the weight and mass were kept constant.
3. It was observed that stiffness of the structure increases with increasing the number of unit cells as well as decreasing the unit cell sizes.
4. Decreasing the number of unit cells while the volume and mass were kept constant resulted in higher energy absorption and less deformation under similar amount of applied force.

References

[1] X.Z. Zhang, M. Leary, H.P. Tang, T. Song, M. Qian, Selective electron beam manufactured Ti-6Al-4V lattice structures for orthopedic implant applications: Current status and outstanding challenges, Curr. Opin. Solid State Mater. Sci. 22 (2018) 75–99. doi:10.1016/j.cossms.2018.05.002.

[2] M. Dallago, V. Fontanari, B. Winiarski, F. Zanini, S. Carmignato, M. Benedetti, Fatigue properties of Ti6Al4V cellular specimens fabricated via SLM: CAD vs real geometry, Procedia Struct. Integr. 7 (2017) 116–123. doi:10.1016/j.prostr.2017.11.068.
[3] I. Ullah, M. Brandt, S. Feih, Failure and energy absorption characteristics of advanced 3D truss core structures, Mater. Des. 92 (2016) 937–948. doi:10.1016/j.matdes.2015.12.058.
[4] T. Tancogne-Dejean, A.B. Spierings, D. Mohr, Additively-manufactured metallic micro-lattice materials for high specific energy absorption under static and dynamic loading, Acta Mater. 116 (2016) 14–28. doi:10.1016/j.actamat.2016.05.054.
[5] W.S.W. Harun, M.S.I.N. Kamariah, N. Muhamad, S.A.C. Ghani, F. Ahmad, Z. Mohamed, A review of powder additive manufacturing processes for metallic biomaterials, Powder Technol. 327 (2018) 128–151. doi:10.1016/j.powtec.2017.12.058.
[6] C.M. Haslauer, J.C. Springer, O.L.A. Harrysson, E.G. Loboa, N.A. Monteiro-Riviere, D.J. Marcellin-Little, In vitro biocompatibility of titanium alloy discs made using direct metal fabrication, Med. Eng. Phys. 32 (2010) 645–652. doi:10.1016/j.medengphy.2010.04.003.
[7] M. Leary, M. Mazur, J. Elambasseril, M. McMillan, T. Chirent, Y. Sun, M. Qian, M. Easton, M. Brandt, Selective laser melting (SLM) of AlSi12Mg lattice structures, Mater. Des. 98 (2016) 344–357. doi:10.1016/j.matdes.2016.02.127.
[8] L. Xiao, W. Song, Additively-manufactured functionally graded Ti-6Al-4V lattice structures with high strength under static and dynamic loading: Experiments, Int. J. Impact Eng. 111 (2018) 255–272. doi:10.1016/j.ijimpeng.2017.09.018.
[9] I. Maskery, N.T. Aboulkhair, A.O. Aremu, C.J. Tuck, I.A. Ashcroft, Compressive failure modes and energy absorption in additively manufactured double gyroid lattices, Addit. Manuf. 16 (2017) 24–29. doi:10.1016/j.addma.2017.04.003.
[10] A. Yánez, A. Herrera, O. Martel, D. Monopoli, H. Afonso, Compressive behaviour of gyroid lattice structures for human cancellous bone implant applications, Mater. Sci. Eng. C. 68 (2016) 445–448. doi:10.1016/j.msec.2016.06.016.
[11] Q. Feng, Q. Tang, Y. Liu, R. Setchi, S. Soe, S. Ma, L. Bai, Quasi-static analysis of mechanical properties of Ti6Al4V lattice structures manufactured using selective laser melting, Int. J. Adv. Manuf. Technol. (2017) 2301–2313. doi:10.1007/s00170-017-0932-7.
[12] A. du Plessis, I. Yadroitsava, I. Yadroitsev, Ti6Al4V lightweight lattice structures manufactured by laser powder bed fusion for load-bearing applications, Opt. Laser Technol. 108 (2018) 521–528. doi:10.1016/j.optlastec.2018.07.050.
[13] A. Ataee, Y. Li, D. Fraser, G. Song, C. Wen, Anisotropic Ti-6Al-4V gyroid scaffolds manufactured by electron beam melting (EBM) for bone implant applications, Mater. Des. 137 (2018) 345–354. doi:10.1016/j.matdes.2017.10.040.
[14] A. Yánez, A. Cuadrado, O. Martel, H. Afonso, D. Monopoli, Gyroid porous titanium structures: A versatile solution to be used as scaffolds in bone defect reconstruction, Mater. Des. 140 (2018) 21–29. doi:10.1016/j.matdes.2017.11.050.
[15] R. Shrestha, A. Sterling, B. Lessel, N. Phan, M. Reza, V. Sereshk, N. Shamsaei, Mechanical Behavior of Additively Manufactured 17-4 PH Stainless Steel Schoen Gyroid Lattice Structure, in: Solid Free. Fabr., 2018: pp. 716–723.
[16] C. Yan, L. Hao, A. Hussein, D. Raymont, Evaluations of cellular lattice structures manufactured using selective laser melting, Int. J. Mach. Tools Manuf. 62 (2012) 32–38. doi:10.1016/j.ijmachtools.2012.06.002.

[17] B. Van Hooreweder, J.P. Kruth, Advanced fatigue analysis of metal lattice structures produced by Selective Laser Melting, CIRP Ann. - Manuf. Technol. 66 (2017) 221–224. doi:10.1016/j.cirp.2017.04.130.
[18] K. Lietaert, A. Cutolo, D. Boey, B. Van Hooreweder, Fatigue life of additively manufactured Ti6Al4V scaffolds compression and compression- compression fatigue load, Sci. Rep. (2018) 1–9. doi:10.1038/s41598-018-23414-2.
[19] C. Yan, L. Hao, A. Hussein, P. Young, D. Raymont, Advanced lightweight 316L stainless steel cellular lattice structures fabricated via selective laser melting, Mater. Des. 55 (2014) 533–541. doi:10.1016/j.matdes.2013.10.027.
[20] L. Yang, R. Mertens, M. Ferrucci, C. Yan, Y. Shi, S. Yang, Continuous graded Gyroid cellular structures fabricated by selective laser melting: Design, manufacturing and mechanical properties, Mater. Des. 162 (2019) 394–404. doi:10.1016/j.matdes.2018.12.007.
[21] M. Ashby, Hybrid materials to expand the boundaries of material-property space, J. Am. Ceram. Soc. 94 (2011). doi:10.1111/j.1551-2916.2011.04559.x.
[22] J.Y. Rho, R.B. Ashman, C.H. Turner, Young's modulus of trabecular and cortical bone material: Ultrasonic and microtensile measurements, J. Biomech. (1993). doi:10.1016/0021-9290(93)90042-D.